


Quantum remote implementation with polarization-temporal hyperentanglement

Meiyu Wang^{1,3}, Hao Guo^{1,3}, Fengli Yan^{1,3,*} and Ting Gao^{2,†}

¹College of Physics, Hebei Normal University, Shijiazhuang 050024, China

²School of Mathematics Science, Hebei Normal University, Shijiazhuang 050024, China

³Hebei Key Laboratory of Photophysics Research and Application, Shijiazhuang 050024, China

 (Received 5 June 2023; revised 31 August 2023; accepted 11 September 2023; published 5 October 2023)

Remote implementation of quantum operation between two distant nodes is crucial for many quantum applications. Here we consider the implementation of an arbitrary single-photon operation upon a remote quantum system exploiting photon pairs simultaneously entangled in the polarization and temporal degrees of freedom, which is a fascinating resource in long-distance quantum communication with its outstanding merits. To improve the level of security for the above protocol, we also consider a controlled implementation of quantum operation scenario by adding a supervisor, which is necessary for distributed quantum computation in a quantum network. Both of the protocols can be fulfilled by bidirectional state teleportation with the aid of the effective cross-Kerr interaction. Furthermore, the simple construction circuits together with available existing optical elements and common single-photon detectors facilitate the realization of our protocols with current sufficient technologies.

DOI: [10.1103/PhysRevApplied.20.044016](https://doi.org/10.1103/PhysRevApplied.20.044016)

I. INTRODUCTION

Remote implementation of quantum operation (RIO) is a crucial component for building scalable quantum networks. The application of RIO plays a crucial role in long-distance quantum information processing and communication tasks, such as distributed quantum computation [1,2], blind quantum computation [3,4], and quantum program [5,6]. Similar to conventional quantum state teleportation (QST) [7], RIO can transmit a quantum operation of the sender from a local quantum system and apply on a remote receiver's state through a pre-established entangled channel, local operations and classical communication. Thus we also refer to it as quantum operation teleportation. In 2001, Huelga *et al.* [8] proposed the remote implementation of a quantum operation in the case of one qubit. Such a RIO protocol can be fulfilled by bidirectional quantum state teleportation (BQST) consuming two bits of entanglement (e bits) plus four bits of classical information (c bits), which is the maximum total amount of required resource. In the same year, the remote implementation of a controlled NOT (CNOT) operation was given by the authors of Ref. [9] using one e bit and two c bits. Next, Huelga *et al.* [10] showed that the single-qubit operators belonging to one of the two restricted sets can be remotely implemented with the same overall resource as that needed in Ref. [9].

Here, those operations that belong to some restricted sets are usually called partially unknown operations. Indeed, the resource cost in the remote implementations of partially unknown quantum operations is significantly fewer than that consumed in the remote implementations of completely unknown quantum operations. In addition, the remote implementations of partially unknown quantum operations can satisfy the requirements of some practical applications. Considering these advantages, it is very useful to investigate the extension of RIO to the cases of multiqubits. In 2006, Wang [11] developed the idea of RIO and proposed the RIO protocol for partially unknown quantum operations of multiqubits belonging to restricted sets. Moreover, the experimental implementation scheme in the cavity QED has been considered [12]. In 2007, Wang also put forward a combined and controlled RIO scheme for partially unknown quantum operations with Greenberger-Horne-Zeilinger (GHZ) states [13]. Since then, a series of works on RIO have appeared and made some interesting progresses. For example, Chen and Hwang [14] studied multiparty RIO of single-qubit partially unknown operations based on a shared entanglement of GHZ states. In 2014, Chen and Lu [15] proposed a protocol for multiparty remote implementation of quantum rotation via partially entangled quantum channels. Soon after, Hu *et al.* [16] discussed the remote implementation of a three-qubit Toffoli gate via optical microcavities. In 2018, Lv *et al.* [17] presented the joint remote control of an arbitrary single-qubit operation with multiparticle entangled states. Recently, RIO in quantum multihop networks has also been

*flyan@mail.hebtu.edu.cn

†gaoting@mail.hebtu.edu.cn

presented by Wu *et al.* [18]. In experiment, teleporting a CNOT operation [19] and a rotation angle [20] have been demonstrated.

In recent years, there has been great interest in using entangled photons as quantum resources for quantum information processing tasks. Particularly, hyperentangled state [21], which means photons are simultaneously entangled in multiple degrees of freedom (DOFs), has captured much attention. To date, the use of various photonic DOFs and hyperentangled states has already shown advantages in optical quantum computing [22–24] and quantum communication, such as state discrimination [25–29], entanglement concentration and purification [30–36], entanglement distribution [37,38], superdense teleportation [39, 40], quantum key distribution [41], and quantum secure direction communication [42,43]. Diverse kinds of hyperentangled states in different DOFs have been demonstrated through the processes of waveguide-based spontaneous parametric down-conversion, e.g., polarization-spatial [44], polarization-frequency [45], polarization-momentum [46], polarization-time-bin [47], and polarization-orbital angular momentum [48].

Based on a polarization-spatial hyperentangled Bell state, Jiao *et al.* [49] have proposed a developmental RIO protocol, where the sender implements an arbitrary single-qubit operation upon the remote partner's quantum state encoded in the path DOF. As we all know, the polarization of the photon is the most popular DOF since it is easy to manipulate with current technology. Although the spatial mode is also easy to operate, measure, and distinguish with linear optical elements, each photon requires two paths during the transmission, which will cause the circuit to become more complicated in long-distance multiphoton communication. Particularly in the case of transmitting photons using optical fibers, where two paths of photons merge into one path, the temporal DOF of photons with two different times of arrival as the basis is now a much better choice. In this paper, we propose a feasible RIO protocol with the polarization-temporal hyperentangled Bell state. In order to improve the level of security for the above RIO proposal, we also consider a RIO scenario by adding a supervisor acting as a controller who has the right to decide on completion of the RIO task. Controlled remote implementation of operator (CRIO) is a key multipartite extension of bipartite quantum remote control, which becomes an integral part of the design of quantum networks. Both of the two tasks can be fulfilled in two steps by BQST. First, the polarization-DOF part of the maximally polarization-temporal hyperentangled Bell (GHZ) state is exploited to transfer the state encoded in the polarization DOF from one node, Alice, to another remote node, Bob, so that Bob can implement the general operator on it. Second, Bob applies the temporal-DOF part of the quantum channel to transfer his state to Alice. With the conversion technique using some optical elements,

Alice can get the desired target state in the polarization DOF.

The rest of this paper is organized as follows. In Sec. II, we introduce our RIO protocol using the hyperentangled Bell state in polarization and temporal DOFs in detail. Section III investigates the controlled RIO with the polarization-temporal hyperentangled GHZ state. We discuss the success probability and feasibility on the practical RIO (CRIO) in Sec. IV. Finally, we make a discussion and conclusion in Sec. V.

II. RIO PROTOCOL EXECUTION WITH THE POLARIZATION-TEMPORAL HYPERENTANGLED BELL STATE

Before our protocol, let us first simply review the experimental method of producing polarization and temporal-entangled photons by using nondegenerate spontaneous parametric down-conversion [40,41]. As shown in Fig. 1, an 80-MHz mode-locked 532-nm laser with a pulse width of about 7 ps is sent through an unbalanced Mach-Zehnder interferometer (MZI) to split each pulse into two time bins, the early and late pulse, separated by 2.4 ns. After the MZI, the polarization of the pump beam is prepared using wave plates, then the pump is directed into a polarizing Sagnac interferometer (PSI) with a dichroic mirror (DM) that is highly reflective for the pump and highly transmissive for the signal (idler) output. The PSI [50,51] consists of a polarizing beam splitter (PBS), a periodically poled lithium niobate (PPLN) crystal, a Fresnel rhomb, and a calcite crystal. PBS transmits the horizontal state and reflects the vertical one. After PBS, the horizontal (vertical) pump component traverses the interferometer clockwise (counterclockwise) and undergoes type-0 phase-matched SPDC inside the PPLN crystal, resulting in a pair of horizontally polarized photons (the signal photon and the idler photon) with wavelengths 810 and 1550 nm, respectively. The Fresnel rhomb, acting as a broadband half-wave plate (HWP), causes the output of the clockwise path to be vertically polarized, and hence polarization entanglement has been prepared. A 4.1-cm piece of calcite crystal in the PSI (after the transmitted port of the PBS) is used for temporal compensation, to cancel the wavelength-dependent delay of the Fresnel rhomb. For more information on this generation setup, see Refs. [40,41]. And hence, this Sagnac polarization entangled photon source produce the hyperentangled state in polarization and time bin

$$|\psi\rangle_{AB} = \frac{1}{2}(|Ht_1\rangle_{810}|Ht_1\rangle_{1550} + |Vt_1\rangle_{810}|Vt_1\rangle_{1550} + |Ht_2\rangle_{810}|Ht_2\rangle_{1550} + |Vt_2\rangle_{810}|Vt_2\rangle_{1550}), \quad (1)$$

where $|H\rangle$ ($|V\rangle$) refers to the horizontally (vertically) polarized photon state, t_1 and t_2 denote two time bins, the

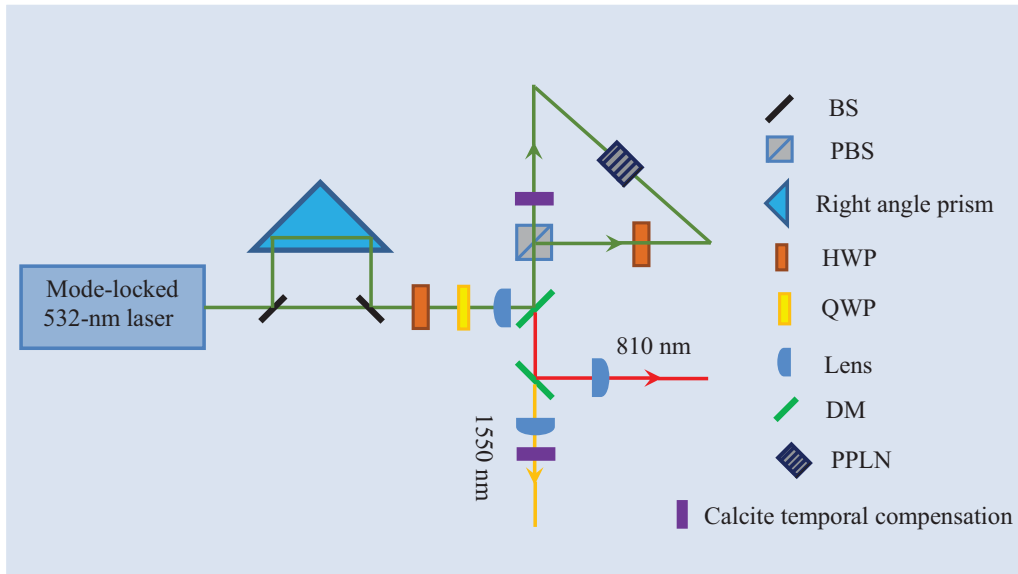


FIG. 1. Optical setup for generation of time-bin and polarization entanglement via SPDC in the Sagnac polarization-entanglement source. Green lines denote the 532-nm pump (and stabilization) beam, red and yellow represent the signal (810 nm) and idler (1550 nm) photons, respectively. BS, beam splitter; PBS, polarizing beam splitter; HWP, half-wave plate; QWP, quarter-wave plate; DM, dichroic mirror; PPLN, periodically poled lithium niobate.

early and the late arrival time of a photon. The two wavelengths of photons are 810 and 1550 nm, respectively. So far, a few of quantum communication applications using time-bin and polarization-entangled photons have been achieved, such as superdense teleportation [40], high-dimensional quantum key distribution [41], remote preparation of time-encoded single-photon states [52–54], and nonlocality verification [55].

In the following, we will consider the RIO protocol adopting the polarization-temporal hyperentangled state in Eq. (1), which can be rewritten as

$$\begin{aligned} |\psi\rangle_{AB} &= |\psi^P\rangle_{AB} |\psi^T\rangle_{AB} \\ &= \frac{1}{\sqrt{2}}(|HH\rangle + |VV\rangle)_{AB} \otimes \frac{1}{\sqrt{2}}(|t_1 t_1\rangle + |t_2 t_2\rangle)_{AB}, \end{aligned} \quad (2)$$

where the superscripts P and T stand for the polarization and time-bin DOF, respectively. Photon A is owned by Alice while photon B belongs to Bob. Alice has another photon A_1 in the polarization-DOF state $|\phi\rangle = \delta|H\rangle + \eta|V\rangle$ with $|\delta|^2 + |\eta|^2 = 1$. Bob's goal is to send a general unitary operation U_B to Alice and help her transform the state $|\phi\rangle$ to $U_B|\phi\rangle = \delta'|H\rangle + \eta'|V\rangle$. Initially, the state of the three photons can be written as

$$\begin{aligned} |\Phi_0\rangle_{A_1 AB} &= |\phi\rangle_{A_1} \otimes |\psi\rangle_{AB} \\ &= (\delta|HHH\rangle + \delta|HVV\rangle + \eta|VHH\rangle \\ &\quad + \eta|VVV\rangle)_{A_1 AB} \otimes (|t_1 t_1\rangle + |t_2 t_2\rangle)_{AB}. \end{aligned} \quad (3)$$

For lightening the mathematical formulation, we omit the normalization coefficients of formula (3). We will also ignore any common factors in all of the following formula. As illustrated in Fig. 2, the RIO task consists of two main procedures. The first procedure is the application of polarization entanglement and cross-Kerr effect, while the temporal-DOF part of the quantum channel is exploited in the second procedure.

Figure 2(a) shows a schematic diagram of the first step consisting of four noncentrosymmetric (NCS) calcite crystals, two Kerr nonlinear media, and two wave plates. A pair of NCS calcite crystals acts as the beam displacer and the beam combiner, respectively. Calcite beam displacers are used to orientate the photon into the lower or upper path in terms of the polarization states of the photon, and calcite beam combiners can recombine the two arms of the photon. After photons (A_1, A) pass through the first beam displacer, one arm of each qubit interacts with the coherence state $|\alpha_1\rangle$ via the first Kerr medium, with a further linear phase shifter and the first beam combiner, the state of the system composed of three photons and the probe light evolves to

$$\begin{aligned} |\Phi_1\rangle_{n\theta, \text{Kerr1}} &= (\delta|HHH\rangle + \eta|VVV\rangle)_{A_1 AB} |\alpha_1\rangle \\ &\quad + \delta|HVV\rangle_{A_1 AB} |\alpha_1 e^{-i\theta}\rangle \\ &\quad + \eta|VHH\rangle_{A_1 AB} |\alpha_1 e^{i\theta}\rangle. \end{aligned} \quad (4)$$

Here we do not write the time-bin entanglement part to evade unnecessary cumbersomeness. This equation indicates there are two results corresponding to the phase shifts

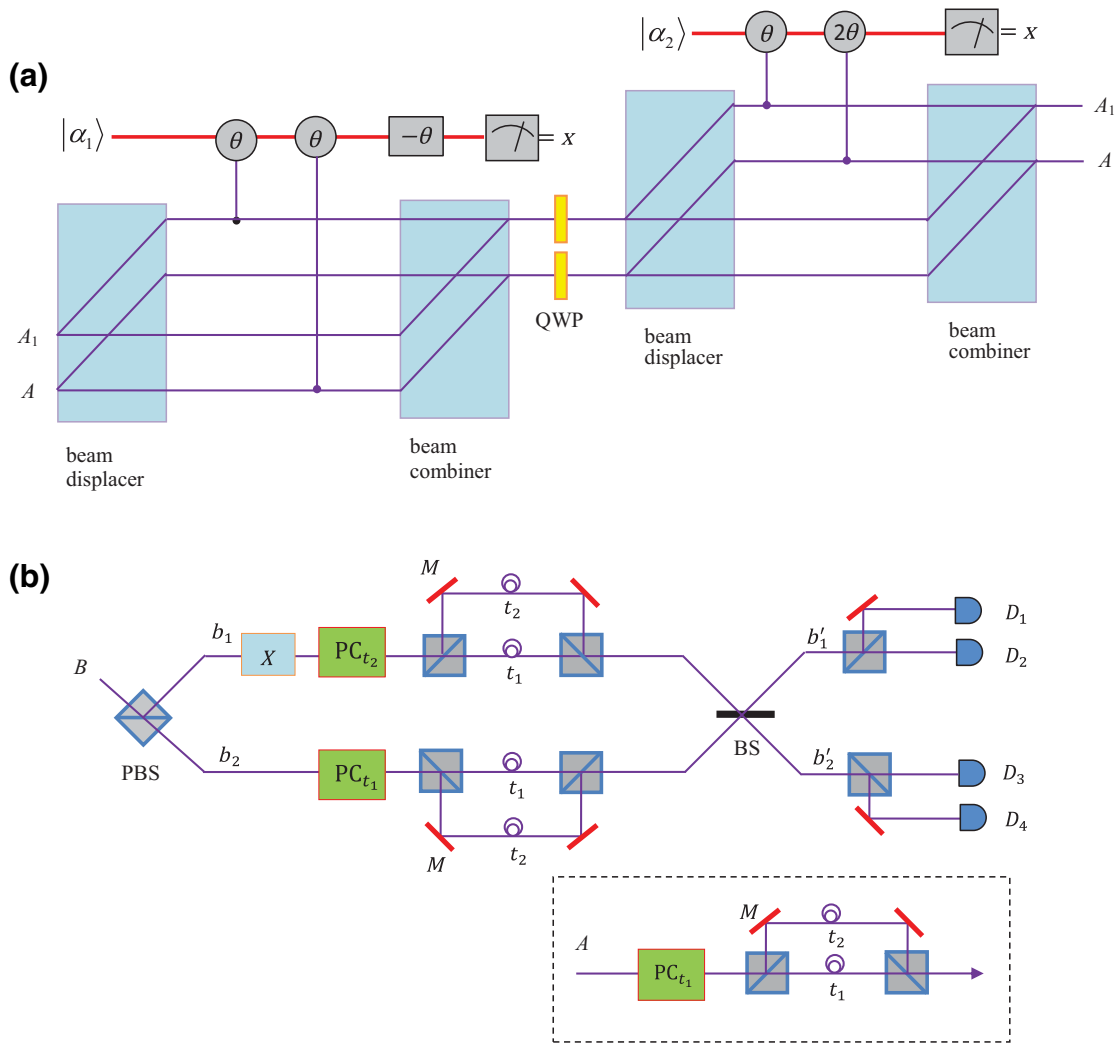


FIG. 2. A schematic diagram of the RIO protocol with polarization and time-bin DOFs. (a) The physical implementation of the first procedure. Initially, the state of photon A_1 is encoded in polarization DOF. The calcite beam displacer orients photons A_1A into either the upper or lower path based on their polarization modes. The calcite beam combiner, which can recombine the two paths, is the same as the calcite beam displacer, only rotated by 90° to keep the symmetry of the two paths. (b) The physical implementation of the second procedure. X is a NOT gate on the time-bin state. PC is a Pockels cell, which can perform polarization bit-flip operation corresponding to arrival time of the photons. D_i is the common single-photon detector. The optical circle on the different path denotes time delay t_1 or t_2 .

$\pm n\theta$, ($n = 0, 1$) if an X -quadrature measurement is performed on the coherent state. It needs to be noted that the phase shift $\pm\theta$ are not be distinguished from each other, but a classical feed-forward operation can eliminate the phase shift [56,57]. The probability of misidentifying $|\alpha\rangle$ as $|\alpha e^{\pm i\theta}\rangle$ is depicted by the complementary error function $\frac{1}{2}\text{erfc}[\alpha(1 - \cos\theta)/\sqrt{2}]$, which is less than 10^{-5} with a constraint condition $\alpha\theta^2 \sim 9$.

The cross-Kerr nonlinearity has been studied extensively and has well-known applications in numerous optical quantum information processing [58–66]. In light of this, over the past years, there have been many theoretical and experimental studies endeavoring to generate the fantastically strong interactions to implement a Kerr

nonlinearity. So far, a large cross-Kerr phase shifts up to $13 \mu\text{rad}/\text{photon}$ [67], $0.3 \text{ mrad}/\text{photon}$ [68], and $3 \text{ mrad}/\text{polariton}$ [69] have been reported. Particularly, methods using electromagnetically induced transparency [70–72] or sequential photon-atom interactions [73,74] achieve π -phase shift using microsecond pulse sequences and milliwatt ancillary beams. These experimental results are promising not only for the development of nonlinear optics but also for applications in information processing and transmission based on cross-phase modulation.

To simplify description in the later processes, we take the scenario of zero phase shift as a representative example. In this case, three photons are in the state $|\Phi_2\rangle_{A_1AB} = (\delta|HHH\rangle + \eta|VVV\rangle)_{A_1AB}$. Two QWPs are placed into the

TABLE I. The relations between X -quadrature measurement results of two coherent probe beams, the final polarization state of photon B , and Bob's feed-forward operations, where $Z^P = |H\rangle\langle H| - |V\rangle\langle V|$ and $X^P = |H\rangle\langle V| + |V\rangle\langle H|$.

| Measurement of $ \alpha_1\rangle$ | Measurement of $ \alpha_2\rangle$ | Polarization state of B | Feed forward on B |
|------------------------------------|-----------------------------------|------------------------------------|---------------------|
| $ \alpha_1\rangle$ | $ \alpha_2\rangle$ | $\delta H\rangle + \eta V\rangle$ | None |
| $ \alpha_1\rangle$ | $ \alpha_2 e^{i\theta}\rangle$ | $\delta H\rangle - \eta V\rangle$ | Z^P |
| $ \alpha_1\rangle$ | $ \alpha_2 e^{i2\theta}\rangle$ | $\delta H\rangle - \eta V\rangle$ | Z^P |
| $ \alpha_1\rangle$ | $ \alpha_2 e^{i3\theta}\rangle$ | $\delta H\rangle + \eta V\rangle$ | None |
| $ \alpha_1 e^{\pm i\theta}\rangle$ | $ \alpha_2\rangle$ | $\delta V\rangle + \eta H\rangle$ | X^P |
| $ \alpha_1 e^{\pm i\theta}\rangle$ | $ \alpha_2 e^{i\theta}\rangle$ | $\delta V\rangle - \eta H\rangle$ | $Z^P X^P$ |
| $ \alpha_1 e^{\pm i\theta}\rangle$ | $ \alpha_2 e^{i2\theta}\rangle$ | $-\delta V\rangle + \eta H\rangle$ | $Z^P X^P$ |
| $ \alpha_1 e^{\pm i\theta}\rangle$ | $ \alpha_2 e^{i3\theta}\rangle$ | $-\delta V\rangle - \eta H\rangle$ | X^P |

paths of photons (A_1, A) to implement the Hadamard transformation, i.e., $|H\rangle \rightarrow \frac{1}{\sqrt{2}}(|H\rangle + |V\rangle)$, $|V\rangle \rightarrow \frac{1}{\sqrt{2}}(|H\rangle - |V\rangle)$. Subsequently, photon A_1 and A pass through the second beam displacer, the second Kerr medium and interact with the coherence state $|\alpha_2\rangle$, as a result, the state of the whole system can be expressed as

$$\begin{aligned}
 |\Phi_3\rangle_{m\theta, \text{Kerr}2} = & |HH\rangle_{A_1 A} (\delta|H\rangle + \eta|V\rangle)_B |\alpha_2\rangle \\
 & + |VH\rangle_{A_1 A} (\delta|H\rangle - \eta|V\rangle)_B |\alpha_2 e^{i\theta}\rangle + \\
 & + |HV\rangle_{A_1 A} (\delta|H\rangle - \eta|V\rangle)_B |\alpha_2 e^{i2\theta}\rangle \\
 & + |VV\rangle_{A_1 A} (\delta|H\rangle + \eta|V\rangle)_B |\alpha_2 e^{i3\theta}\rangle. \quad (5)
 \end{aligned}$$

After the X -quadrature measurement is performed on the coherent state $|\alpha_2\rangle$, there exist four groups of measurement outcomes corresponding to four scenarios of phase shifts $m\theta$ ($m = 0, 1, 2, 3$). When Alice sends her measurement outcomes to Bob, who then performs some classical feed-forward operations, so that the original state $|\phi\rangle$ can be reconstructed on photon B . For the other results of X -quadrature measurements on two coherent states $|\alpha_1\rangle$ and $|\alpha_2\rangle$, the similar description is omitted because of space

and clarity. Table I lists the relations between X -quadrature measurement results of two coherent probe beams, the final polarization state of photon B , and Bob's feed-forward operations.

In the following, the second procedure of RIO begins after Bob implements a general unitary operation U_B on photon B , as a result, $U_B|\phi\rangle = \delta'|H\rangle + \eta'|V\rangle$. It is worth mentioning that the feed-forward operations applied on photon B at the end of the first step can be absorbed by U_B . Without loss of generality, we assume the alternative state of photons (A, B) including the time-bin-DOF part is

$$|\Phi_4\rangle_{AB} = |H\rangle_A (\delta'|H\rangle + \eta'|V\rangle)_B \otimes (|t_1 t_1\rangle + |t_2 t_2\rangle)_{AB}. \quad (6)$$

The second RIO schematic setup is shown in Fig. 2(b). X is a NOT gate on the time-bin state, which can be completed by the active switches [75]. The PC_{t_i} ($i = 1, 2$) refers to the Pockels cell (PC) [76], which is used to flip the polarizations of photon B when the time is t_i . Each MZI composed of a pair of PBSs can adjust the time-bin state such that the optical path-length difference between the two arms cancels the time difference between the two time bins. The state that arrives at the BS evolves as

$$\begin{aligned}
 |\Phi_5\rangle_{AB} = & \delta'|H^{t_1}\rangle_A |H^{t_1}\rangle_B + \delta'|H^{t_2}\rangle_A |H^{t_2}\rangle_B + \eta'|H^{t_1}\rangle_A |V^{t_1}\rangle_B + \eta'|H^{t_2}\rangle_A |V^{t_2}\rangle_B \\
 \xrightarrow{\text{PBS}} & \delta'|H^{t_1}\rangle_A |H^{t_1}\rangle_{b_2} + \delta'|H^{t_2}\rangle_A |H^{t_2}\rangle_{b_2} + \eta'|H^{t_1}\rangle_A |V^{t_1}\rangle_{b_1} + \eta'|H^{t_2}\rangle_A |V^{t_2}\rangle_{b_1} \\
 \xrightarrow{X} & \delta'|H^{t_1}\rangle_A |H^{t_1}\rangle_{b_2} + \delta'|H^{t_2}\rangle_A |H^{t_2}\rangle_{b_2} + \eta'|H^{t_1}\rangle_A |V^{t_2}\rangle_{b_1} + \eta'|H^{t_2}\rangle_A |V^{t_1}\rangle_{b_1} \\
 \xrightarrow{\text{PCs}} & \delta'|H^{t_1}\rangle_A |V^{t_1}\rangle_{b_2} + \delta'|H^{t_2}\rangle_A |H^{t_2}\rangle_{b_2} + \eta'|H^{t_1}\rangle_A |H^{t_2}\rangle_{b_1} + \eta'|H^{t_2}\rangle_A |V^{t_1}\rangle_{b_1} \\
 \xrightarrow{\text{MZIs}} & \delta'|H^{t_1}\rangle_A |V^{t_1+t_2}\rangle_{b_2} + \delta'|H^{t_2}\rangle_A |H^{t_2+t_1}\rangle_{b_2} + \eta'|H^{t_1}\rangle_A |H^{t_2+t_1}\rangle_{b_1} + \eta'|H^{t_2}\rangle_A |V^{t_1+t_2}\rangle_{b_1}. \quad (7)
 \end{aligned}$$

It is obvious that the time interval between the two time bins of photon B does not exist, so we will omit it in subsequent expression.

Under the operation of a polarization preserving 50: 50 BS and by dropping the global phase, we obtain

$$\begin{aligned}
|\Phi_6\rangle_{AB} &= |H\rangle_{b'_1}(\delta'|H^2\rangle + \eta'|H^1\rangle)_A + |V\rangle_{b'_1}(\delta'|H^1\rangle + \eta'|H^2\rangle)_A \\
&\quad + |H\rangle_{b'_2}(\eta'|H^1\rangle - \delta'|H^2\rangle)_A + |V\rangle_{b'_2}(\eta'|H^2\rangle - \delta'|H^1\rangle)_A \\
&= |H\rangle_{b'_1}|\phi'_1\rangle_A + |V\rangle_{b'_1}|\phi'_2\rangle_A + |H\rangle_{b'_2}|\phi'_3\rangle_A + |V\rangle_{b'_2}|\phi'_4\rangle_A.
\end{aligned} \tag{8}$$

At the terminals, Bob measures photon B with four photodetectors D_1, D_2, D_3, D_4 . When either photodetector clicks, photon A is projected onto one of the group $\{|\phi'_1\rangle_A, |\phi'_2\rangle_A, |\phi'_3\rangle_A, |\phi'_4\rangle_A\}$, which is encoded in the temporal DOF. So Alice should perform a series of conversion operations from the temporal DOF to the polarization DOF, as illustrated in the dotted box of Fig. 2(b). Finally, the precisely target state, $(\delta'|H\rangle + \eta'|V\rangle)_A$, is obtained by applying one of the Pauli operators. Therefore, Bob successfully implements a general unitary operation U_B on Alice's quantum state $|\phi\rangle$.

III. CRIO VIA POLARIZATION-TEMPORAL HYPERENTANGLED GHZ STATE

CRIO is similar to the standard RIO protocol with an added step. The objective is Bob implements an arbitrary single-qubit operation upon Alice's quantum system only with the permission of the controller, Charlie. Suppose Alice, Bob, and Charlie share a polarization-temporal hyperentangled GHZ state of the form

$$\begin{aligned}
|\psi^{PT}\rangle_{ABC} &= |\psi^P\rangle_{ABC}|\psi^T\rangle_{ABC}, \\
|\psi^P\rangle_{ABC} &= |H\rangle_A|H\rangle_B|H\rangle_C + |V\rangle_A|V\rangle_B|V\rangle_C, \quad (9) \\
|\psi^T\rangle_{ABC} &= |t_1\rangle_A|t_1\rangle_B|t_1\rangle_C + |t_2\rangle_A|t_2\rangle_B|t_2\rangle_C.
\end{aligned}$$

Initially, the total state of photons (A_1, A, B, C) is written as

$$\begin{aligned}
|\Phi_0\rangle_{A_1ABC} &= |\phi\rangle_{A_1} \otimes |\psi^{PT}\rangle_{ABC} \\
&= (\delta|HHHH\rangle + \delta|HVVV\rangle + \eta|VHHH\rangle \\
&\quad + \eta|VVVV\rangle)_{A_1ABC} \otimes (|t_1t_1t_1\rangle + |t_2t_2t_2\rangle)_{ABC}.
\end{aligned} \tag{10}$$

Similar to the case of RIO described in Sec. II, this task can also be completed in two steps. In the first step, since Alice performs the same operations as in Fig. 2(a), hence, this process is omitted here. At the same time, the temporal-DOF part of the quantum channel will be put aside until when the second step starts. Now assume that, after two X -quadrature measurements on the coherent states $|\alpha_1\rangle$ and $|\alpha_2\rangle$, the collapsed state is

$$|\Phi'_2\rangle_{ABC} = |H\rangle_A(\delta|HH\rangle + \eta|VV\rangle)_{BC}. \tag{11}$$

Clearly, photon A is no longer entangled with photons (B, C) in the polarization-DOF part. To control the task,

Charlie will apply some operations as in Fig. 3(a). The resulting state is

$$\begin{aligned}
|\Phi'_3\rangle_{\beta, \text{Kerr}} &= |H\rangle_A(\delta|H\rangle + \eta|V\rangle)_B|H\rangle_C|\beta\rangle \\
&\quad + |H\rangle_A(\delta|H\rangle - \eta|V\rangle)_B|V\rangle_C|\beta e^{i\theta}\rangle.
\end{aligned} \tag{12}$$

Being performed an X -quadrature measurement on the coherent state $|\beta\rangle$, photon C is disentangled from photon B . For simplifying the description in the later processes, we shall take the zero-phase shift for example, so we may obtain the three-photon state $|H\rangle_A(\delta|H\rangle + \eta|V\rangle)_B|H\rangle_C$. Subsequently, Bob applies the operation U_B on photon B , adding the temporal-DOF part $|\psi^T\rangle_{ABC}$, the entire system is

$$\begin{aligned}
|\Phi'_4\rangle_{ABC} &= |H\rangle_A(\delta'|H\rangle + \eta'|V\rangle)_B|H\rangle_C \otimes (|t_1\rangle_A|t_1\rangle_B|t_1\rangle_C \\
&\quad + |t_2\rangle_A|t_2\rangle_B|t_2\rangle_C).
\end{aligned} \tag{13}$$

Now the second step begins with Bob's operations shown in Fig. 2(b). These operations transform $|\Phi'_4\rangle_{ABC}$ to

$$\begin{aligned}
|\Phi'_5\rangle_{ABC} &= |H\rangle_{b'_1}(\eta'|H^1\rangle_A|H^1\rangle_C + \delta'|H^2\rangle_A|H^2\rangle_C) \\
&\quad + |V\rangle_{b'_1}(\delta'|H^1\rangle_A|H^1\rangle_C + \eta'|H^2\rangle_A|H^2\rangle_C)
\end{aligned}$$

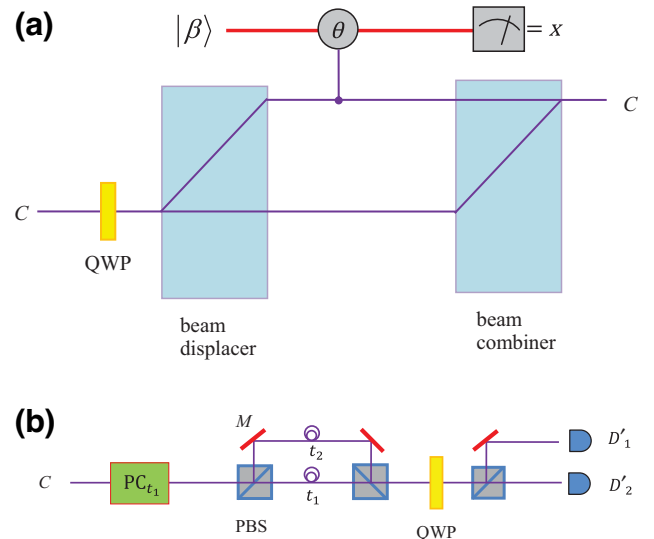


FIG. 3. Charlie's operation in the whole CRIO process. (a) Charlie's operation in the first step of CRIO. (b) Charlie's operation in the second step of CRIO.

$$\begin{aligned}
 &+ |H\rangle_{b'_2}(\eta'|H^1\rangle_A|H^1\rangle_C - \delta'|H^2\rangle_A|H^2\rangle_C) \\
 &+ |V\rangle_{b'_2}(\eta'|H^2\rangle_A|H^2\rangle_C - \delta'|H^1\rangle_A|H^1\rangle_C).
 \end{aligned} \tag{14}$$

If either of four detectors fires, photon B will be disentangled from photons (A, C) and we should forget it from now on. Assume that the collapsed state is $\delta'|H^1\rangle_A|H^1\rangle_C + \eta'|H^2\rangle_A|H^2\rangle_C$, Charlie again exercises his power as a controller by executing what is shown in Fig. 3(b). By doing so, the state of photons A and C changes to

$$\begin{aligned}
 |\Phi'_6\rangle_{AC} = &|H\rangle_C(\delta'|H^1\rangle + \eta'|H^2\rangle)_A \\
 &+ |V\rangle_C(\eta'|H^2\rangle - \delta'|H^1\rangle)_A.
 \end{aligned} \tag{15}$$

Upon measurement, Charlie sends his results to Alice, correspondingly, Alice should perform a series of conversion operations from the temporal DOF to the polarization DOF, as illustrated in the dotted box of Fig. 2(b). Finally, with X^P or $X^P Z^P$, the precisely target state is obtained, and hence the RIO task involving Alice and Bob is completed with Charlie's permission.

IV. CHARACTERIZATION OF THE RIO (CRIO)

A. Effect resulting from photon dissipation of the coherent state

When an X -quadrature measurement is performed in the RIO (CRIO) process, it is necessary to analyze the effect resulting from photon dissipation of the coherent state, which can not be avoided. The model of photon dissipation could be described by the standard master equation [77]

$$\frac{\partial \rho(t)}{\partial t} = \gamma a \rho(t) a^\dagger - \frac{\gamma}{2} [a^\dagger a \rho(t) + \rho(t) a^\dagger a], \tag{16}$$

where $\rho(t)$ stands for the density matrix of the system, a (a^\dagger) denotes the annihilation (creation) operator of the probe mode. The decay constant γ quantifies the dissipation of the coherent state.

With the solving method adopted in Ref. [61], after performing the first X -quadrature measurement on the dissipated coherent state $|\alpha_1\rangle$, the error probability is modified to $\frac{1}{2} \operatorname{erfc}[A\alpha_1(1 - \cos\theta)/\sqrt{2}]$ with $A = e^{-\gamma/2t}$. While when detecting the second position quadrature X of the dissipated coherent state $|\alpha_2\rangle$, there are four Gaussian functions $f(x, A\alpha_2 \cos n\theta) = (2\pi)^{-1/4} \exp[-\frac{1}{4}(x - 2A\alpha_2 \cos n\theta)^2]$, $n = 0, 1, 2, 3$. The partial overlap between two adjacent Gaussian curves induces a measurement

error rate $\varepsilon_i = \frac{1}{2} \operatorname{erfc}(x_{d_j}/2\sqrt{2})$ with $x_{d_j} = 2A\alpha_2[\cos j\theta - \cos(j+1)\theta]$, $j = 0, 1, 2$. Since the overlap between the two adjacent curves of $n = 0, 1$ is much bigger than that between the other two neighboring curves with $n = 1, 2$, or $n = 2, 3$, so we consider only the error probability caused by the tiny overlap between the two adjacent curves with $n = 0, 1$. Therefore, under the condition that the initial amplitudes of both the coherent states are the same, the success probability of our RIO protocol by applications of two X -quadrature measurements is calculated by

$$P_{\text{suc}} = (1 - P_{\text{err}})^2 = \left\{1 - \frac{1}{2} \operatorname{erfc}[A\alpha(1 - \cos\theta)/\sqrt{2}]\right\}^2. \tag{17}$$

For CRIO, this success probability is $(1 - P_{\text{err}})^3$. In Fig. 4, we plot the success probability of our RIO (CRIO) proposal when the following physical parameters are set: the phase shift, $\theta = \pi$ rad, the initial amplitude of all used coherent states, $0 \leq \alpha \leq 1$, and the decoherence factor A ranging from 0 to 1. It is easy to see that the success probability can be improved by increasing the original amplitude α and decreasing the photon dissipation γ of the coherent state. Particularly, the success probability changing with the decoherence factor A under the condition of $\alpha = 1$ is shown in Fig. 4(b). Based on the analyses above, the success probability of practical RIO (CRIO) can be achieved satisfying the current attainable cross-Kerr phase shifts, low-intensity coherent states and weak-decoherence environment.

B. Effect resulting from a real single-photon detector

The effect resulting from the efficiency of a real single-photon detector also needs to be considered. Two main parameters, the quantum efficiency η and the dark count rate λ , are important for characterizing the performance of the real detector. In general, the dark counts approximately follow the Poisson distribution [78,79], therefore, during the measurement interval τ , we can give the distribution probability of having d dark counts as $P(d) = (\lambda\tau)^d/d! e^{-\lambda\tau}$. Furthermore, the conditional probability of responding to k -photon events when l photons are presented is calculated by

$$P(k|l) = \sum_{d=0}^k C_l^d P(k-d)\eta^d(1-\eta)^{l-d}. \tag{18}$$

The success probability of our RIO (CRIO) protocol at the final detection stage is thus written as

$$P'_{\text{suc}} = \begin{cases} P(1|1)P(0|0)^3 = e^{-3\lambda\tau}[\lambda\tau e^{-\lambda\tau}(1-\eta) + e^{-\lambda\tau}\eta], & \text{for RIO,} \\ P(1|1)^2P(0|0)^6 = e^{-6\lambda\tau}[\lambda\tau e^{-\lambda\tau}(1-\eta) + e^{-\lambda\tau}\eta]^2, & \text{for CRIO.} \end{cases} \tag{19}$$

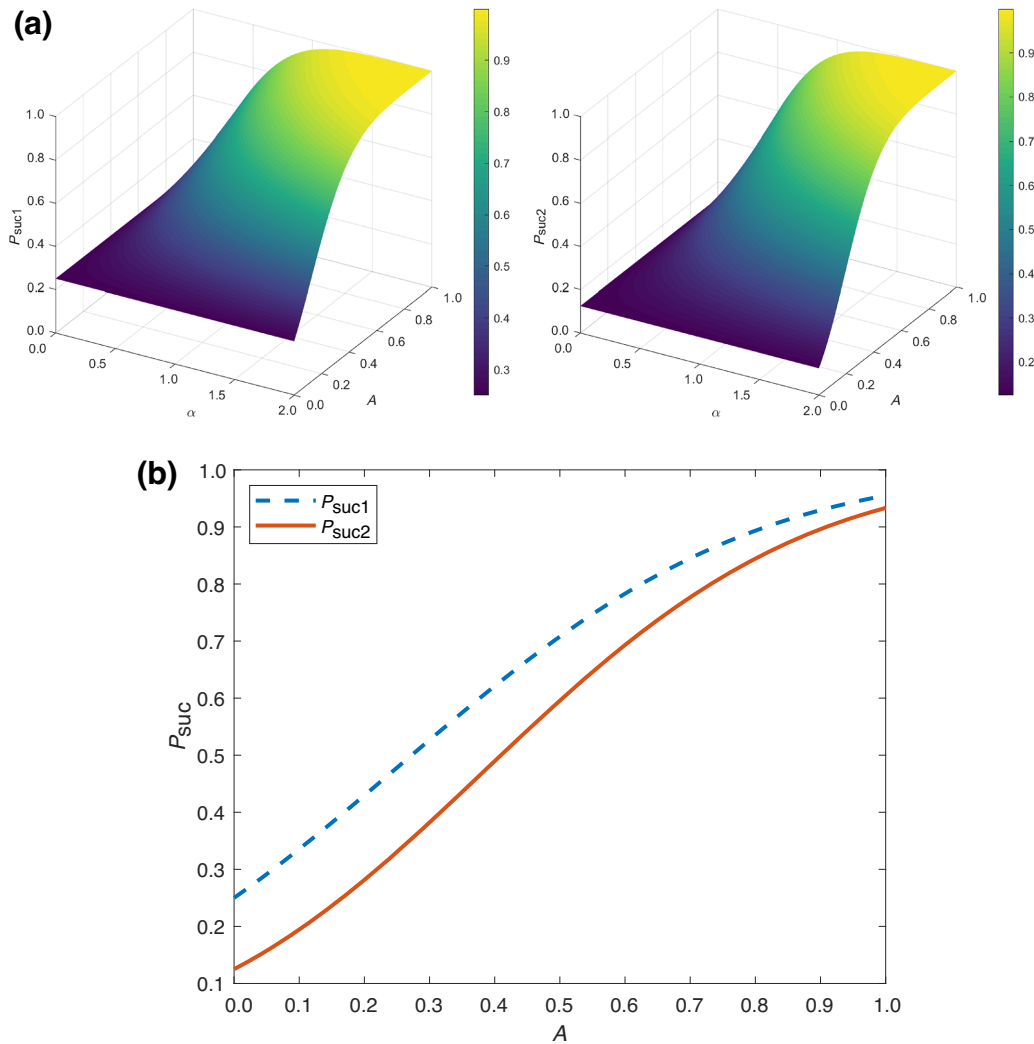


FIG. 4. Illustration plots of the success probabilities considering photon dissipation of the coherent state with the phase shift being set $\theta = \pi$ rad. (a) The curved surface where the success probabilities P_{suc1} (RIO) and P_{suc2} (CRIO) vary with the initial amplitude α of the coherent state and the decoherence factor A . (b) The success probability changes with A under the condition of $\alpha = 1$.

At present, among non-photon-number-resolving detectors, the ultrasensitivity avalanche photodiodes (APDs) have been widely used in the field of long-distance quantum communication due to their advantages of high quantum efficiency, low dark counts, and room-temperature operation. For Si-APD, the quantum efficiency can reach 0.6–0.8 and the dark count rate is 0.1 kHz. Assume that $\eta = 0.8$, $\lambda\tau = 10^{-7}$, then the probability of a successful readout for the proposed RIO (CRIO) is $P'_{\text{suc1}} = 0.8$ ($P'_{\text{suc2}} = 0.64$).

V. DISCUSSION AND CONCLUSION

The remote implementation of quantum operation is closely associated with nonlocal quantum operations through local implementation. RIO or CRIO will thus be helpful for the design of distributed quantum computing

within a quantum network, among which some quantum computers located at different places are connected and the remote implementations of quantum communication and computations are performed over all the relevant quantum nodes. In this paper, we have investigated remote implementation of a general operator between two nodes enabled by Kerr media, hyperentangled states, available existing optical elements, and mature single-photon detection techniques. This optical RIO task can be completed in two steps. In the first step, with the aid of cross-Kerr interaction and X homodyne measurements of the coherent states, the state encoded in the polarization DOF is transferred from Alice to Bob via the polarization-DOF part of the hyperentanglement so that Bob can implement the general operator on it. In the second step, using available optical elements and common single-photon detectors, Bob exploits the temporal-DOF part of the hyperentanglement

to teleport his state to Alice. With the conversion technique using some optical elements, Alice can get the desired target state in the polarization DOF. To raise security and increase variety, we have also considered a controlled RIO scenario, which is a key multipartite extension of bipartite RIO. Moreover, CRIO becomes the fundamental component of a large-scale practical quantum communication network that could form the backbone of the future quantum internet.

Considering a realistic condition, we analyze the effect resulting from photon dissipation of the coherent state and the efficiency of a real single-photon detector. Both results show that our method has potential to complete the RIO tasks. Meanwhile, the time-of-flight difference of the MZI and the current Pockels cells can meet the requirement for the order of a few nanoseconds, which is much less than the time of fluctuation in the fiber. It should be pointed out that here we do not take into account the imperfection of the optical elements, such as PBS, BS, HWP, and QWP, which may decrease the fidelity of the input state. For example, when the photons enter the calcite beam displacer (combiner), the deviation of mirror mounts and the polarization extinction ratio of the calcite beam displacer (combiner) will deviate the real quantum state from the original input state. We will investigate the effect from the inevitable imperfection of these optical elements in our future work. Alternatively, it is interesting and significant to discuss parallel RIO of partially unknown operations on photon state simultaneously encoded in both polarization-DOF and temporal-DOF since it contains high capacity long-distance quantum information processing and communication. We will study these in the future.

ACKNOWLEDGMENTS

This work was funded by the National Natural Science Foundation of China under Grants No. 62271189, No. 11805050, and No. 12071110, Hebei Natural Science Foundation of China under Grant No. A2022205004, Hebei Central Guidance on Local Science and Technology Development Foundation of China under Grant No. 236Z7604G, Science and Technology Project of Hebei Education Department under Grant No. ZD2021066, and Science Foundation of Hebei Normal University under Grant No. L2021B13.

-
- [1] J. I. Cirac, A. K. Ekert, S. F. Huelga, and C. Macchiavello, Distributed quantum computation over noisy channels, *Phys. Rev. A* **59**, 4249 (1999).
 - [2] J. Eisert, K. Jacobs, P. Papadopoulos, and M. B. Plenio, Optimal local implementation of nonlocal quantum gates, *Phys. Rev. A* **62**, 052317 (2000).
 - [3] A. M. Childs, Secure assisted quantum computation, *Quantum Inf. Comput.* **5**, 456 (2005).

- [4] Q. Li, W. H. Chan, C. H. Wu, and Z. H. Wen, Triple-server blind quantum computation using entanglement swapping, *Phys. Rev. A* **89**, 040302 (2014).
- [5] M. A. Nielsen and I. L. Chuang, Programmable quantum gate arrays, *Phys. Rev. Lett.* **79**, 321 (1997).
- [6] A. Sørensen and K. Mølmer, Error-free quantum communication through noisy channels, *Phys. Rev. A* **58**, 2745 (1998).
- [7] C. H. Bennett, G. Brassard, C. Crépeau, R. Jozsa, A. Peres, and W. K. Wootters, Teleporting an unknown quantum state via dual classical and Einstein-Podolsky-Rosen channels, *Phys. Rev. Lett.* **70**, 1895 (1993).
- [8] S. F. Huelga, J. A. Vaccaro, A. Cheffles, and M. B. Plenio, Quantum remote control: Teleportation of unitary operations, *Phys. Rev. A* **63**, 042303 (2001).
- [9] D. Collins, N. Linden, and S. Popescu, Nonlocal content of quantum operations, *Phys. Rev. A* **64**, 032302 (2001).
- [10] S. F. Huelga, M. B. Plenio, and J. A. Vaccaro, Remote control of restricted sets of operations: Teleportation of angles, *Phys. Rev. A* **65**, 042316 (2002).
- [11] A. M. Wang, Remote implementations of partially unknown quantum operations of multiqubits, *Phys. Rev. A* **74**, 032317 (2006).
- [12] Q. Liang and A. M. Wang, Scheme for remote implementation of partially unknown quantum operation of two qubits in cavity QED, *Commun. Theor. Phys.* **50**, 1233 (2008).
- [13] A. M. Wang, Combined and controlled remote implementations of partially unknown quantum operations of multiqubits using Greenberger-Horne-Zeilinger states, *Phys. Rev. A* **75**, 062323 (2007).
- [14] Y. T. Chen and T. Hwang, Multiparty quantum remote control, *Quantum Inf. Process.* **12**, 3545 (2013).
- [15] L. B. Chen and H. Lu, Deterministic and controlled many-to-one and one-to-many remote quantum rotations via partially entangled quantum channels, *Sci. China Ser. G Phys. Mech. Astron.* **44**, 187 (2014).
- [16] S. Hu, W. X. Cui, D. Y. Wang, C. H. Bai, Q. Guo, H. F. Wang, A. D. Zhu, and S. Zhang, Teleportation of a Toffoli gate among distant solid-state qubits with quantum dots embedded in optical microcavities, *Sci. Rep.* **5**, 11321 (2015).
- [17] S. X. Lv, Z. W. Zhao, and P. Zhou, Joint remote control of an arbitrary single-qubit state by using a multipartite entangled state as the quantum channel, *Quantum Inf. Process.* **17**, 8 (2018).
- [18] F. Wu, L. Tang, M. Q. Bai, and Z. W. Mo, Remote implementation of quantum operations in quantum multihop networks, *J. Opt. Soc. Am. B* **39**, 2813 (2022).
- [19] Y. F. Huang, X. F. Ren, Y. S. Zhang, L. M. Duan, and G. C. Guo, Experimental teleportation of a quantum controlled-NOT gate, *Phys. Rev. Lett.* **93**, 240501 (2004).
- [20] G. Y. Xiang, J. Li, and G. C. Guo, Teleporting a rotation on remote photons, *Phys. Rev. A* **71**, 044304 (2005).
- [21] J. T. Barreiro, N. K. Langford, N. A. Peters, and P. G. Kwiat, Generation of hyperentangled photon pairs, *Phys. Rev. Lett.* **95**, 260501 (2005).
- [22] B. C. Ren, G. Y. Wang, and F. G. Deng, Universal hyperparallel hybrid photonic quantum gates with dipole-induced transparency in the weak-coupling regime, *Phys. Rev. A* **91**, 032328 (2015).

- [23] T. Li and G. L. Long, Hyperparallel optical quantum computation assisted by atomic ensembles embedded in double-sided optical cavities, *Phys. Rev. A* **94**, 022343 (2016).
- [24] W. Q. Liu, H. R. Wei, and L. C. Kwek, Low-cost Fredkin gate with auxiliary space, *Phys. Rev. Appl.* **14**, 054057 (2020).
- [25] T. C. Wei, J. T. Barreiro, and P. G. Kwiat, Hyperentangled Bell-state analysis, *Phys. Rev. A* **75**, 060305 (2007).
- [26] Y. B. Sheng, F. G. Deng, and G. L. Long, Complete hyperentangled-Bell-state analysis for quantum communication, *Phys. Rev. A* **82**, 032318 (2010).
- [27] N. Pisenti, C. P. E. Gaebler, and T. W. Lynn, Distinguishability of hyperentangled Bell states by linear evolution and local projective measurement, *Phys. Rev. A* **84**, 022340 (2011).
- [28] X. H. Li and S. Ghose, Self-assisted complete maximally hyperentangled state analysis via the cross-Kerr nonlinearity, *Phys. Rev. A* **93**, 022302 (2016).
- [29] G. Y. Wang, B. C. Ren, F. G. Deng, and G. L. Long, Complete analysis of hyperentangled Bell states assisted with auxiliary hyperentanglement, *Opt. Express* **27**, 8994 (2019).
- [30] X. H. Li and S. Ghose, Hyperentanglement concentration for time-bin and polarization hyperentangled photons, *Phys. Rev. A* **91**, 062302 (2015).
- [31] M. Y. Wang, J. Z. Xu, F. L. Yan, and T. Gao, Entanglement concentration for polarization-spatial-time-bin hyperentangled Bell states, *EPL* **123**, 60002 (2018).
- [32] G. L. Jiang, W. Q. Liu, and H. R. Wei, Heralded and high-efficient entanglement concentrations based on linear optics assisted by time-delay degree of freedom, *Opt. Express* **30**, 47836 (2022).
- [33] G. L. Jiang, W. Q. Liu, and H. R. Wei, Practically enhanced hyperentanglement concentration for polarization-spatial hyperentangled Bell states with linear optics and common single-photon detectors, *Phys. Rev. Appl.* **19**, 034044 (2023).
- [34] S. Ecker, P. Sohr, L. Bulla, M. Huber, M. Bohmann, and R. Ursin, Experimental single-copy entanglement distillation, *Phys. Rev. Lett.* **127**, 040506 (2021).
- [35] Y. B. Sheng and F. G. Deng, Deterministic entanglement purification and complete nonlocal Bell-state analysis with hyperentanglement, *Phys. Rev. A* **81**, 032307 (2010).
- [36] X. M. Hu, C. X. Huang, Y. B. Sheng, L. Zhou, B. H. Liu, Y. Guo, C. Zhang, W. B. Xing, Y. F. Huang, C. F. Li, and G. C. Guo, Long-distance entanglement purification for quantum communication, *Phys. Rev. Lett.* **126**, 010503 (2021).
- [37] N. L. Piparo, W. J. Munro, and K. Nemoto, Quantum multiplexing, *Phys. Rev. A* **99**, 022337 (2019).
- [38] X. M. Hu, W. B. Xing, B. H. Liu, D. Y. He, H. Cao, Y. Guo, C. Zhang, H. Zhang, Y. F. Huang, C. F. Li, and G. C. Guo, Efficient distribution of high-dimensional entanglement through 11 km fiber, *Optica* **7**, 738 (2020).
- [39] T. M. Graham, H. J. Bernstein, T. C. Wei, M. Junge, and P. G. Kwiat, Superdense teleportation using hyperentangled photons, *Nat. Commun.* **6**, 7185 (2015).
- [40] J. C. Chapman, T. M. Graham, C. K. Zeitler, H. J. Bernstein, and P. G. Kwiat, Time-bin and polarization superdense teleportation for space applications, *Phys. Rev. Appl.* **14**, 014044 (2020).
- [41] J. C. Chapman, C. C. W. Lim, and P. G. Kwiat, Hyperentangled time-bin and polarization quantum key distribution, *Phys. Rev. Appl.* **18**, 044027 (2022).
- [42] S. S. Chen, L. Zhou, W. Zhong, and Y. B. Sheng, Three-step three-party quantum secure direct communication, *Sci. China Phys. Mech. Astron.* **61**, 090312 (2018).
- [43] Y. B. Sheng, L. Zhou, and G. L. Long, One-step quantum secure direct communication, *Sci. Bull.* **67**, 367 (2022).
- [44] T. Yang, Q. Zhang, J. Zhang, J. Yin, Z. Zhao, M. Zukowski, Z. B. Chen, and J. W. Pan, All-versus-nothing violation of local realism by two-photon, four-dimensional entanglement, *Phys. Rev. Lett.* **95**, 240406 (2005).
- [45] A. Yabushita and T. Kobayashi, Spectroscopy by frequency-entangled photon pairs, *Phys. Rev. A* **69**, 013806 (2004).
- [46] M. Barbieri, C. Cinelli, P. Mataloni, and F. De Martini, Polarization-momentum hyperentangled states: realization and characterization, *Phys. Rev. A* **72**, 052110 (2005).
- [47] C. Schuck, G. Huber, C. Kurtsiefer, and H. Weinfurter, Complete deterministic linear optics bell state analysis, *Phys. Rev. Lett.* **96**, 190501 (2006).
- [48] D. Bhatti, J. von Zanthier, and G. S. Agarwal, Entanglement of polarization and orbital angular momentum, *Phys. Rev. A* **91**, 062303 (2015).
- [49] X. F. Jiao, P. Zhou, and S. X. Lv, Remote implementation of single-qubit operations via hyperentangled states with cross-Kerr nonlinearity, *J. Opt. Soc. Am. B* **36**, 867 (2019).
- [50] B. S. Shi and A. Tomita, Generation of a pulsed polarization entangled photon pair using a Sagnac interferometer, *Phys. Rev. A* **69**, 013803 (2004).
- [51] T. Kim, M. Fiorentino, and F. N. C. Wong, Phase-stable source of polarization-entangled photons using a polarization Sagnac interferometer, *Phys. Rev. A* **73**, 012316 (2006).
- [52] A. Zavatta, M. D'Angelo, V. Parigi, and M. Bellini, Remote preparation of arbitrary time-encoded single-photon ebits, *Phys. Rev. Lett.* **96**, 020502 (2006).
- [53] M. Y. Wang, Y. H. Zheng, L. X. Fu, F. L. Yan, and T. Gao, Remote preparation of a general single-photon hybrid state, *Results Phys.* **27**, 104497 (2021).
- [54] M. Y. Wang, F. L. Yan, and T. Gao, Remote preparation for single-photon state in two degrees of freedom with hyperentangled states, *Front. Phys.* **16**, 41501 (2021).
- [55] C. K. Zeitler, J. C. Chapman, E. Chitambar, and P. G. Kwiat, Entanglement verification of hyperentangled photon pairs, *Phys. Rev. Appl.* **18**, 054025 (2022).
- [56] K. Nemoto and W. J. Munro, Nearly deterministic linear optical controlled-NOT gate, *Phys. Rev. Lett.* **93**, 250502 (2004).
- [57] T. P. Spiller, K. Nemoto, S. L. Braunstein, W. J. Munro, P. van Loock, and G. J. Milburn, Quantum computation by communication, *New J. Phys.* **8**, 30 (2006).
- [58] F. G. Deng, Efficient multipartite entanglement purification with the entanglement link from a subspace, *Phys. Rev. A* **84**, 052312 (2011).
- [59] F. G. Deng, Optimal nonlocal multipartite entanglement concentration based on projection measurements, *Phys. Rev. A* **85**, 022311 (2012).

- [60] Y. B. Sheng, L. Zhou, S. M. Zhao, and B. Y. Zheng, Efficient single-photon-assisted entanglement concentration for partially entangled photon pairs, *Phys. Rev. A* **85**, 012307 (2012).
- [61] L. Dong, J. X. Wang, Q. Y. Li, H. Z. Shen, H. K. Dong, X. M. Xiu, Y. J. Gao, and C. H. Oh, Nearly deterministic preparation of the perfect W state with weak cross-Kerr nonlinearities, *Phys. Rev. A* **93**, 012308 (2016).
- [62] X. M. Xiu, Q. Y. Li, Y. F. Lin, H. K. Dong, L. Dong, and Y. J. Gao, Preparation of four-photon polarization-entangled decoherence-free states employing weak cross-Kerr nonlinearities, *Phys. Rev. A* **94**, 042321 (2016).
- [63] M. Y. Wang, Q. Z. Hao, F. L. Yan, and T. Gao, Simultaneous qubit-loss-free fusion of three multiple W states, *Laser Phys. Lett.* **15**, 055201 (2018).
- [64] K. Fukui, M. Endo, W. Asavanant, A. Sakaguchi, J. Yoshikawa, and A. Furusawa, Generating the Gottesman-Kitaev-Preskill qubit using a cross-Kerr interaction between squeezed light and Fock states in optics, *Phys. Rev. A* **105**, 022436 (2022).
- [65] L. Dong, S. L. Wang, C. Cui, X. Geng, Q. Y. Li, H. K. Dong, X. M. Xiu, and Y. J. Gao, Polarization Toffoli gate assisted by multiple degrees of freedom, *Opt. Lett.* **43**, 4635 (2018).
- [66] R. Yanagimoto, T. Onodera, E. Ng, L. G. Wright, P. L. McMahon, and H. Mabuchi, Engineering a kerr-based deterministic CBIC phase gate via Gaussian operations, *Phys. Rev. Lett.* **124**, 240503 (2020).
- [67] A. Feizpour, M. Hallaji, G. Dmochowski, and A. M. Steinberg, Observation of the nonlinear phase shift due to single post-selected photons, *Nat. Phys.* **11**, 905 (2015).
- [68] V. Venkataraman, K. Saha, and A. L. Gaeta, Phase modulation at the few-photon level for weak-nonlinearity-based quantum computing, *Nat. Photonics* **7**, 138 (2013).
- [69] T. Kuriakose, P. M. Walker, T. Dowling, O. Kyriienko, I. A. Shelykh, P. St-Jean, N. C. Zambon, A. Lemaître, I. Sagnes, L. Legrati, A. Harouri, S. Ravets, M. S. Skolnick, A. Amo, J. Bloch, and D. N. Krizhanovskii, Few-photon all-optical phase rotation in a quantum-well micropillar cavity, *Nat. Photonics* **16**, 566 (2022).
- [70] Z. Y. Liu, Y. H. Chen, Y. C. Chen, H. Y. Lo, P. J. Tsai, I. A. Yu, Y. C. Chen, and Y. F. Chen, Large cross-phase modulations at the few-photon level, *Phys. Rev. Lett.* **117**, 203601 (2016).
- [71] D. Tiarks, S. Schmidt, G. Rempe, and S. Dürr, Optical π phase shift created with a single-photon pulse, *Sci. Adv.* **2**, e1600036 (2016).
- [72] S. S. Stophel, R. Shahrokhshahi, B. Jordaán, M. Namazi, and E. Figueroa, Conditional π -phase shift of single-photon-level pulses at room temperature, *Phys. Rev. Lett.* **125**, 243601 (2020).
- [73] B. Hacker, S. Welte, G. Rempe, and S. Ritter, A photon-photon quantum gate based on a single atom in an optical resonator, *Nature* **536**, 193 (2016).
- [74] S. Sun, H. Kim, Z. Luo, G. S. Solomon, and E. Waks, A single-photon switch and transistor enabled by a solid-state quantum memory, *Science* **361**, 57 (2018).
- [75] Y. Soudagar, F. Bussi eres, G. Berlin, S. Lacroix, J. M. Fernandez, and N. Godbout, Cluster-state quantum computing in optical fibers, *J. Opt. Soc. Am. B* **24**, 226 (2007).
- [76] D. Kalamidas, Single-photon quantum error rejection and correction with linear optics, *Phys. Lett. A* **343**, 331 (2005).
- [77] S. Phoenix, Wave-packet evolution in the damped oscillator, *Phys. Rev. A* **41**, 5132 (1990).
- [78] D. Shin, A. Kirmani, V. K. Goyal, and J. H. Shapiro, Photon-efficient computational 3-D and reflectivity imaging with single-photon detectors, *IEEE Trans. Comput. Imaging* **1**, 112 (2015).
- [79] H. Y. Meng, Deterministic linear-optical quantum control gates utilizing path and polarization degrees of freedom, *Phys. Rev. A* **105**, 032607 (2022).